Bio-Design and Manufacturing (2020) 3:48–59
https://doi.org/10.1007/s42242-020-00058-8

RESEARCH ARTICLE

Bioprinting and in vitro characterization of alginate dialdehyde–gelatin hydrogel bio-ink

Fu You[1] · Xia Wu[1] · Michael Kelly[2] · Xiongbiao Chen[1,3]

Received: 28 September 2019 / Accepted: 15 January 2020 / Published online: 23 January 2020

Abstract

Cell-laden cardiac patches have recently been emerging to renew cellular sources for myocardial infarction (MI, commonly know as a heart attack) repair. However, the fabrication of cell-laden patches with porous structure remains challenging due to the limitations of currently available hydrogels and existing processing techniques. The present study utilized a bioprinting technique to fabricate hydrogel patches and characterize them in terms of printability, mechanical and biological properties. Cell-laden hydrogel (or bio-ink) was formulated from alginate dialdehyde (ADA) and gelatin (GEL) to improve the printability, degradability as well as bioactivity. Five groups of hydrogel compositions were designed to investigate the influence of the oxidation degree of ADA and hydrogels concentration on the properties of printed scaffolds. ADA–GEL hydrogels have generally shown favorable for living cells (EA.hy926 cells and hybrid human umbilical vein endothelial cell line). The hydrogel with an oxidation degree of 10% and a concentration ratio of 70/30 (or 10%ADA70–GEL30) demonstrated the best printability among the groups examined. Formulated hydrogels were also bioprinted with the living cells (EA.hy926), and the scaffolds printed were then subject to the cell culture for 7 days. Our results illustrate that the scaffolds bioprinted from 10%ADA70–GEL30 hydrogels had the best homogenous cell distribution and also the highest cell viability. Taken together, in the present study we synthesized a newly formulated bio-ink from ADA and GEL and for the fist time, used them to bioprint cardiac patches, which have the potential to be used in MI repair.

Keywords Bioprinting · Alginate dialdehyde · Gelatin · Bio-ink

Introduction

Myocardial infarction (MI), commonly know as heart attack, results from interruption of the blood supply to a part of the heart, which may lead to heart failure if left untreated. Myocardium will cease to function properly due to the loss of cardiomyocytes after MI, which has an extremely low rate of proliferation (1% for adult mammals [1]) far insufficient to compensate for the loss. This is also accompanied by a cardiac remodeling process due to the formation of scar tissue and degradation of the extracellular matrix (ECM), eventually leading to heart failure [2–6]. Various therapies, including pharmaceutical interventions, have been exploited to slow down the progression to heart failure. Unfortunately, these therapies were not able to restore the function of affected myocardium [7, 8]. Currently, heart transplantation is still the gold standard to treat congestive heart failure, but it is a severely restricted option due to the limited availability of donor organs.

Tissue engineering offers promising alternatives to the above therapies. Currently available cardiac tissue engineering (CTE) techniques mainly include cell-impregnated hydrogel injection and cell-impregnated hydrogel patch implantation, by which cells are delivered into the infarcted heart, serving as renewable cellular sources for MI repair

Electronic supplementary material The online version of this article (https://doi.org/10.1007/s42242-020-00058-8) contains supplementary material, which is available to authorized users.

✉ Xiongbiao Chen
xbc719@mail.usask.ca

[1] Division of Biomedical Engineering, College of Engineering, University of Saskatchewan, Saskatoon, SK S7N 5A9, Canada

[2] Department of Neurosurgery, College of Medicine, University of Saskatchewan, Saskatoon, SK S7N 5A9, Canada

[3] Department of Mechanical Engineering, College of Engineering, University of Saskatchewan, Saskatoon, SK S7N 5A9, Canada

[9–12]. Although cell-impregnated hydrogel injection technique offers advantage like minimally invasive surgery, it has also been reported that most incorporated cells tend to leak from the injection site and drift out of the circulation system. To overcome these issues, cell-impregnated hydrogel patch-based CTE strategies have been shown promising, wherein patches are engineered to mimic the native ECM, thus providing suitable support for the cell delivery to the MI region as well as subsequent cell functions. The ideal engineered patch should be of porous structures made from biocompatible biomaterials (such as hydrogels commonly used nowadays) with living cells and/or bioactive molecules [13].

The present study aimed to employ the emerging extrusion-based bioprinting (EBB) technique to fabricate hydrogel patches for potential MI treatment. Bioprinting refers to the technique that patterns and assembles living cells and biologics in a layer-by-layer deposition process [14, 15]. It allows for building constructs with complex structures with integrity, as well as with mechanical and biological heterogeneity. EBB utilizes the mechanical force generated by air pressure or piston motion to extrude bio-inks (or the mixtures of hydrogel and cells) through nozzles in a controlled manner to fabricate scaffolds of a three-dimensional (3D) structure [14]. EBB has been illustrated promising to fabricate scaffolds with cells of high density and spatial distribution for various tissue engineering application [14, 16–18]. The raw materials to formulate the hydrogels employed in the present study were the alginate (ALG) and gelatin (GEL). ALG is one of the widely used natural biopolymer for bio-inks formulation in EBB due to its fast gelation after printing when exposing to divalent ions [14, 19–21]. However, being inherently non-degradable is the major issue to limit its application in tissue engineering. Although ionically crosslinked ALG hydrogels can be dissolved following the release of the divalent ions crosslinker, the molecular weight of alginate is still higher than the renal clearance threshold of the kidneys and likely, it is not completely being removed out of body [22]. An improved approach to make ALG degradable under physiological conditions is partial oxidation of ALG chains [23], forming alginate dialdehyde (ADA). The oxidization reaction involves cleavage of the carbon–carbon bond and alters the chair conformation to an open-chain adduct containing two aldehyde groups, which enables degradation of the ADA backbone and leads to a reduction in the average molecular weight. In addition, it is also noted that ALG inherently lacks the bioactive ligands necessary for cell adhesion [24]. Appropriate bioactive ligands are essential to promote and regulate cellular behavior and interactions, especially for cell culture and tissue engineering applications [25, 26]. To overcome this issue, modification of ALG with materials containing RGD group to create cell-adhesive ALG has shown promising [24]. In the present study, we used gelatin type A as another component for the bio-ink formulation. Gelatin (GEL) is a biodegradable protein derived from denatured collagen, which transforms the triple helix structure of collagen into a random coil structure containing the cell-interactive RGD-sequences [27, 28]. Meanwhile, it has been reported that GEL and ADA, once mixed, undergo a self-crosslinking process to form covalently crosslinked hydrogels. This forms the basis of the present study to bioprint the mixture of GEL and ADA. Notably, our previous studies [9, 10, 29] have illustrated the self-crosslinked GEL and ADA are suitable for the delivery of living cells and bioactive molecules, by employing the injection technique, for MI treatment. In the present study, we expanded our achievements to synthesize the self-crosslinked GEL and ADA and for the first time, to use them for bioprinting patches for potential cardiac applications, along with the in vitro characterization by examining their printability, mechanical and biological properties.

Materials and methods

Materials

Sodium alginate (from brown algae, medium viscosity, viscosity ≥ 2000 cps of 2% solution at 25 °C), gelatin (type A, Bloom 300, porcine skin) and sodium metaperiodate were obtained from Sigma-Aldrich, USA.

Oxidation of sodium alginate

ADA was synthesized according to a reported method [30]. Briefly, 4.0 g sodium alginate was dispersed into 20 mL ethanol (100%), while different amounts of sodium periodate were solubilized in 20 mL distilled water to obtain periodate solutions with different concentrations. The molar ratios of sodium periodate to a monomeric unit of alginate were set at 5%, 10% and 30%, respectively. Then the sodium periodate solution was slowly mixed into the sodium alginate dispersion, and the mixture was continuously stirred under dark conditions at room temperature. The reaction times were set as 1, 2, 4, 6, 12 and 24 h. Then the reaction was stopped by adding equimolar ethylene glycol (Sigma-Aldrich, USA) with ALG under continuous stirring for another 30 min. The resultant suspension was dialyzed against ultrapure water using a dialysis membrane (MWCO:12400, 99.99%, Sigma-Aldrich, USA) with several changes of water until the dialysate was periodate-free, which was confirmed by the absence of precipitate when adding 0.5 mL of a 1%(w/v) solution of silver nitrate (Fluka Analytical, Switzerland) to 0.5 mL aliquot of the dialysate.

Determination of the oxidation degree

The oxidation degree of ADA was determined by measuring the unconsumed sodium metaperiodate by UV spectrophotometer (UV-1800A, Shimadzu, Japan) using a soluble starch indicator solution [31]. The indicator solution was prepared by mixing equal volumes of 20% (w/v) KI (Sigma, USA) and 1% (w/v) soluble starch solutions (Sigma, USA), using buffer phosphate (pH 7) as a solvent. At each timepoint, 100 µL of the reaction mixture was diluted to 5 mL with deionized water prior to adding the quencher into the reaction. Then 1 mL of the diluted reaction mixture was mixed with 1 mL of indicator solution. The absorbance of the triiodide–starch complex was instantly measured by the UV spectrophotometer at 482 nm. The periodate concentration in the sample was obtained based on a calibration curve calculated from the absorbance of the complex with a known concentration of IO_4^- ($1.26–6.3 \times 10^{-4}$ M). The difference between the initial and final amount of IO_4^- was consumed to react with sodium alginate and oxidized the hydroxyl groups to aldehyde groups.

FTIR analysis

The FTIR spectra were scanned under room temperature with the IlluminatIR II inVia Reflex (Smiths Detection) equipped with an ATR objective (Renishaw). The scanning range is from 650 to 4000 cm^{-1} with a resolution of 4 cm^{-1}. All samples were freeze-dried and ground into powder before the examination.

Rheological analysis

For rheological analysis, the small-amplitude oscillatory shear (SAOS), a main rheological technique to characterize hydrogels, was used [32]. Rheological properties of the ADA–GEL mixture were characterized using a rheometer (AR G2 rheometer, TA Instruments, USA). A cone-plate geometry with a cone diameter of 40 mm and a cone angle of 2° was used, and the measurement gap was fixed at 54 µm. The gelation time at 37 °C was first determined by measurements of the storage (G') and loss (G'') moduli at a constant frequency (1 Hz) and strain (5%) for all groups. Then the hydrogel precursor solution of each group was allowed to be fully crosslinked for an adequate amount of time as determined by the preceding time sweep test in the absence of monitoring. Strain sweep (strain sweeps from 0.01 to 100% at a constant frequency of 1 Hz) and frequency sweep (frequency sweep from 0.01 to 100 Hz at a constant strain of 5%) were performed to verify that all the measurements were done within the viscoelastic region of hydrogels so that the storage (G') and loss (G'') moduli were independent of strain and frequency. For groups that the previously chosen frequency (1 Hz) and strain (5%) were not within the viscoelastic region, a new frequency and strain would be used to redo the time sweep test to determine the gelation time. If the used frequency (1 Hz) and strain (5%) fall within the viscoelastic region of the hydrogel, previous time sweep test results would be unchanged. To investigate the influence of mixture compositions and ADA oxidization on the physical crosslinking of hydrogel solutions, G' and G'' were recorded as a function of the temperature (temperature (37 → 15 °C) at a constant frequency (1 Hz) and strain (5%) for all groups (see Supplementary Table S1).

Crosslinking degree determination

The crosslinking degree of synthesized ADA–GEL hydrogels was determined by ninhydrin assay [33]. One (1) g ADA–GEL hydrogel of each group was heated with 2% (w/v) ninhydrin solution at 100 °C for 20 min. The optical absorbance of the resulting solution was recorded at 570 nm using a UV spectrophotometer. The number of free amino groups in the crosslinked hydrogels which reacted with ninhydrin is proportional to the optical absorbance of the solution. The concentration of free amino groups in the crosslinked hydrogels was determined from a standard curve from the optical absorbance of glycine solutions with different concentrations. ALG–GEL mixture samples were used as a control. The degree of crosslinking was calculated by the following equation:

$$\text{Degree of crosslinking}\,(\%) = \left[(NH_2)\text{nc} - (NH_2)\text{c}\right] / (NH_2)\text{nc} \times 100\%$$

where (NH_2)nc and (NH_2)c are the mole fractions of free amino groups in non-crosslinked and crosslinked samples, respectively.

Scaffold fabrication

The CAD model of the hydrogel construct was designed using Magics Envisiontec (Materialize). The obtained CAD model was then sliced into consecutive layers using bioplotter RP (Envisiontec GmbH). The sliced CAD model was introduced to the interface software (VisualMachine BP, Envisiontec GmbH) controlling the 3D bioplotter system (Envisiontec GmbH) to print scaffolds, which was carried out in a biosafety cabinet.

Prior to fabrication, fresh GEL solution was slowly added to a newly prepared ADA solution, followed by the appropriate amount of stirring time which was determined by preceding rheological analysis for each group to initiate their self-crosslinking processes. Then the pre-crosslinked

ADA–GEL hydrogel was loaded into the LTDH of 3D bioplotter, maintained at 37 °C through the printing process. A plastic cone needle (EFD Nordson) with an internal diameter of 250 μm was used to reach a high resolution. The temperature of the printing surface was controlled at 10 °C to solidify the uncrosslinked GEL in the printed bio-ink during the printing process. 100 mM $CaCl_2$ was used to further crosslink the printed structure for 10 min.

Young's modulus and GEL release of printed hydrogel scaffolds

Young's modulus of each scaffold was determined by applying unconfined compression with a biodynamic mechanical testing machine (Bose) at a rate of 0.01 mm/s immediately after printing. 3D-printed ADA–GEL scaffolds were immersed in PBS at 37 °C and pH of 7.4. At selected time points, the supernatant solution was removed and collected for GEL release analysis. The GEL concentration in the released buffer was determined by colorimetric protein assay by the Lowry method [34], with bovine serum albumin (BSA) as a standard. The absorbance of each solution at 750 nm was measured using a UV spectrophotometer. The release (%) of GEL from the scaffolds was calculated as follows:

$$\text{Gelatin release}\,(\%) = [\text{Gelatin}]_{\text{supernatant}}/[\text{Gelatin}]_{\text{total}} \times 100\%$$

where $[\text{Gelatin}]_{\text{total}}$ is the initial concentration of gelatin (in printed scaffold) and $[\text{Gelatin}]_{\text{supernatant}}$ is the released gelatin concentration in the buffer solution at different time points.

Cell culture

EA.hy926 cells (American Type Culture Collection, Rockville, MD, USA) were kindly provided by Professor Lixin Liu of College of Medicine, University of Saskatchewan. EA.hy926 cells were cultured in DMEM medium (Corning) with L-glutamine, 4.5 g/L glucose and sodium pyruvate, characterized 10% FBS (HyClone), and HAT supplement [sodium hypoxanthine (0.1 mM), aminopterin (0.4 μM) and thymidine (16 μM)] (Gibco), antibiotic–antimycotic (Gibco) and the medium was changed every 2 days. Passage 3–8 EA.hy926 cells were used in the present study. To collect attached EA.hy926 cells, culture flasks were rinsed with PBS and incubated with 0.25% trypsin solution at 37 °C for 5 min. Following the incubation, the culture medium was added to the flask to neutralize the trypsin. The medium was gently pipetted up and down to disperse detached cell in the medium, which was then centrifuged at 300*g* for 5 min to pellet the cells. Collected cell number was determined using a hemocytometer.

Bioprinting cell-laden hydrogel constructs

ADA and GEL solutions were prepared by stir-bar mixing ADA and GEL in PBS under sterile condition, respectively. For each material group, GEL solution was first mixed with ADA solution and the resulted mixture was then mixed with the cell suspension. The final EA.hy926 cells density was 2.7×10^6 cells/mL. All mixing process was done by a three-way stopcock to ensure a homogenous mixing process. To investigate the influence of different hydrogel formulations on cell viability and proliferation, hydrogel disks were made from each hydrogel formulations. A 1-mL syringe was used to inject 150 μL of cell/gel mixture to the well of the culture plate, waited until the mixture evenly covered the bottom of well (usually 15–20 min). 1 mL DMEM was added to each well, followed by 1 mL of autoclaved 100 mM $CaCl_2$ solution for 10 min to further crosslink the hydrogel. This crosslinking medium was then replaced with culture medium, and then the culture plates were cultured in an incubator at 37 °C.

Also, the cell-laden ADA–GEL was loaded into the LTDH of the 3D bioplotter and kept at 37 °C. During bioprinting, the temperature of the printing stage was maintained at 10 °C to accelerate the solidification of printed material. The bioprinting procedure described above was followed to fabricate cell-laden hydrogel constructs. Then the printed cell-laden hydrogel was washed by DMEM for 5 min and cultured in the medium.

Cell viability, proliferation and morphology assessments

The cell viability assay was performed on printed cell-laden hydrogel using the LIVE/DEAD Kit and fluorescence microscopy. At each time point, the culture medium was removed from culture plate wells and the hydrogel was washed with DMEM and stained in 2 mM calcein-AM and 0.5 mM EthD-1 solution in DMEM for 30 min in a 37 °C, 5% CO_2 incubator. The constructs were washed with DMEM twice and imaged using a fluorescence microscope (Leica). To quantitatively determine the cell viability and cell number in the cell-laden constructs, the stained cells were released by incubating the constructs in 300 μL of 1 mg/mL gelatinase, 1 mg/mL alginate in 50 mM EDTA (diluted in DMEM) at 37 °C. The released medium was gently pipetted to obtain an even cell suspension. Samples ($n = 3$) were taken from the cell suspension of each construct and imaged under a coverslip on a standard glass microscope slide at random locations for counting live and dead cells. Cell viability was calculated by the following equation, the number of live cells/(number of live cells + number of dead

cells) × 100%. A hemocytometer was used to count the total cell number in cell suspensions. After 7 days of culture, the EA.hy926 cell-laden hydrogel scaffolds were fixed in 4% paraformaldehyde for 30 min at room temperature. The cell-laden hydrogels were then washed with PBS and treated with 0.1% Triton X-100 for 15 min. 1% Bovine serum albumin was used as the blocker agent for 20 min before the samples were treated with Alexa Fluor 488 phalloidin (1:40) (Abcam) for 90 min. After three times of PBS wash, the samples were then imaged using a confocal laser scanning microscopy.

Results and discussion

Oxidation of ALG

Partial oxidation of ALG by periodate cleaves the vicinal glycols in polysaccharides to form dialdehyde derivatives. Each α-glycol group principally consumes one sodium periodate molecule, and the reaction rate of this process mainly depends on the stereochemistry of the α-glycol group under certain conditions [30, 35]. During the oxidation process, hydroxyl groups linked to the adjacent carbon atoms of the repetitive units are oxidized to form two aldehyde groups in each oxidized monomeric unit by cleaving the carbon–carbon bond. ADA with different oxidation degrees can be obtained by varying the molar ratio of sodium metaperiodate to ALG and in this way, ADA with final oxidization degrees of 5%, 10% and 30% was synthesized. A calibration curve was first calculated from the absorbance of the triiodide–starch complex with a known concentration of $IO4^-$ ($1.26–6.3 \times 10^{-4}$ M) (see Supplementary materials Figure S1). Then the relationship between reaction time and oxidization degree was investigated (see Supplementary materials Table S2). The oxidization yields of 5%, 10% and 30% of groups reached at least 98% after 6 h of oxidization reaction. After 24 h of oxidization reaction, the degree of oxidization of all groups exceeded 99%. Therefore, the time for subsequent oxidization processes of all groups was set at 6 h.

FTIR analysis

ALG and ADA (5%, 10%, 30% oxidized) are characterized by FTIR spectra (Fig. 1). The absorption bands of ALG spectrum at around 1586 and 1385 cm^{-1} are the asymmetric and symmetric stretching peaks of carboxylate salt groups [36]. Other absorption bands reflect the polysaccharide structure of ALG, including 1293 cm^{-1} (C–O stretching), 1016 cm^{-1} (C–O–C stretching) and 1096 cm^{-1} (C–C stretching) [37, 38]. The broad band at around 3278 cm^{-1} of ALG spectrum indicates the presence of –OH groups. When being oxidized, –OH groups stretching vibration become weaker with oxidation degree increases. This is also verified by the intensity ratios of the –OH to the asymmetric –COO stretching vibration (intensity at 3278/1584), which decreases from 0.55 for alginate to 0.50 for 5% oxidized ADA, 0.47 for 10% oxidized ADA and 0.40 for 30% oxidized ADA. However, the symmetric vibration of aldehyde at around 1735 cm^{-1} is not observed in the FTIR spectrum, which could be due to the hemiacetal formation of free aldehyde groups [39].

Rheological characterization of ADA–GEL hydrogel

When working with ADA–GEL hydrogels, the gelation time is first measured by testing the storage (G') and loss (G'') moduli at a constant frequency (1 Hz) and strain (5%) at 37 °C for all groups. Actually, it is difficult to know what SAOS settings (strain amplitude and the frequency) should be used for initial characterization. 1 Hz frequency and 5% strain are chosen here because they are referenced in the literature for similar hydrogels [32]. Gelation time is especially critical since subsequent strain and frequency sweeps need to be conducted on a fully formed or crosslinked hydrogel to determine the linear viscoelastic region.

After obtaining the indicative gelation time for each group, hydrogels are allowed to reach equilibrium for the appropriate amount of time as determined by the preceding time sweep test in the absence of rheological monitoring. A strain sweep from 0.1 to 100% strain is then conducted at a frequency of 1 Hz on the fully formed hydrogel. 5%ADA50–GEL50 shows a long linear behavior of G' and G'' (see Supplementary materials, Figure S2.B); 10%ADA30–GEL70 has a linear strain region up to 10% strain (Figure S3.B); 10%ADA50–GEL50 exhibited a linear region up to 9% strain (Figure S4.B); 10%ADA70–GEL30 has a linear region up to 7% strain (Figure S5.B); and 30%ADA50–GEL50 had a liner strain region up to 50% strain (Figure S6.B). Therefore, 5% strain is an appropriate choice for subsequent sweeps of all groups.

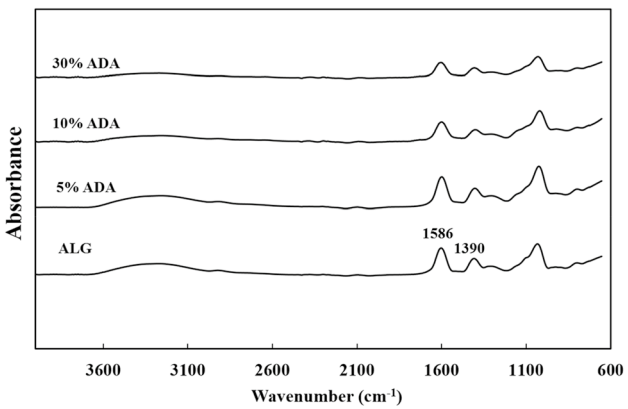

Fig. 1 FTIR spectra of ALG and ADA (5%, 10%, 30% oxidized)

1 Hz frequency was arbitrarily chosen to conduct the initial time sweep test. The results of the frequency sweep using the appropriate strain (as determined in the preceding strain sweep test) allow us to choose a frequency to ensure that the time sweep tests indicate the formation of the hydrogel network rather than some other structural change. Frequency sweeps from 0.1 to 100 Hz were conducted at the 5% strain amplitude determined in the preceding test. For all groups that have been tested, 1 Hz was within the viscoelastic region where storage (G') and loss (G'') moduli are independent of frequency.

Actually, the initial time sweep test conducted employed values of strain (5%) and frequency (1 Hz) that were unverified at the very beginning. It was unclear that if the chosen strain and frequency were suitable enough to be in the viscoelastic region. The strain and frequency sweep performed subsequently established the limits for the viscoelastic region, which confirmed that the strain and frequency chosen for all groups were suitable. The gelation time obtained from the first time sweep reflected the real property of hydrogel network formation. For ADA50–GEL50 groups, gelation time increased with the ADA oxidation degree (Fig. 2a). Higher oxidation degree of ADA normally led to lower viscosity and more aldehyde groups available for covalent crosslinking with amide groups of GEL, which will take longer to form a covalently crosslinked hydrogel. With the same oxidation degree of 10%, the gelation time of ADA–GEL decreased with increasing the ratio of ADA to GEL (Fig. 3b). The first possible reason could be due to that higher concentration of 10% ADA offered more active aldehyde groups than lower concentration groups. This may accelerate the crosslinking efficiency between aldehyde groups and amide groups, and also the hemiacetal formation could consume free aldehyde groups and result in a crosslinking effect.

Last, the temperature sweep test was performed for all groups to determine the physical gelation of hydrogel solutions. The calculated gelation temperature will provide important information for the bioprinting process. The temperature of the bioplotter printing platform can be adjusted to rapidly crosslink printed hydrogel solutions physically according to the tested gelation temperature. It can be observed that all groups showed a gelation temperature above 25 °C. Therefore, the printing platform temperature

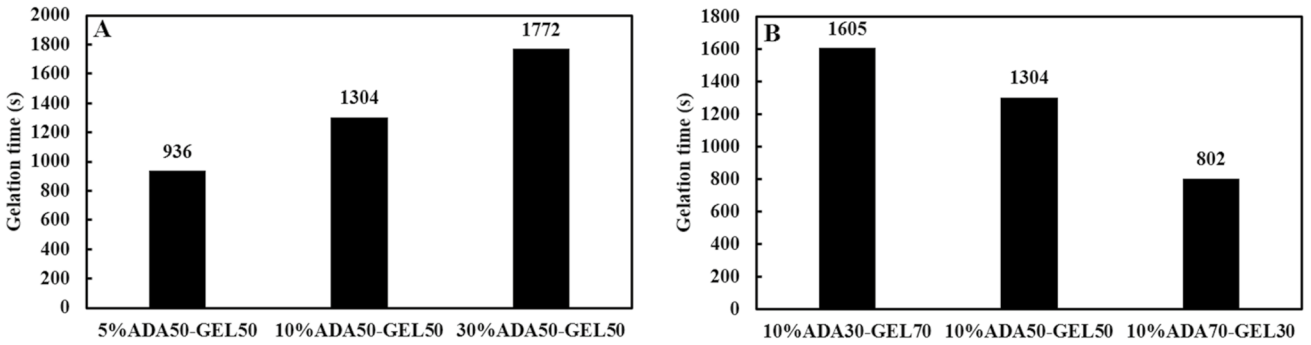

Fig. 2 Gelation time of each group at a constant frequency (1 Hz) and strain (5%): **a** the gelation time of ADA50–GEL50 increases with the ADA oxidation degree, **b** the gelation time of 10% oxidized ADA decreases with the increase in the ratio of ADA/GEL

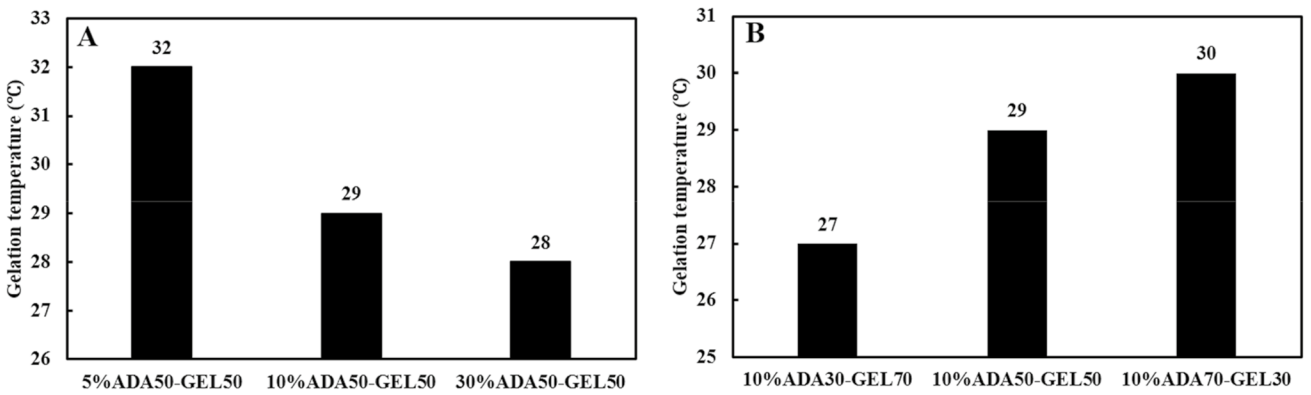

Fig. 3 Gelation temperature of each group at a constant frequency (1 Hz) and strain (5%): **a** the gelation time of ADA50–GEL50 decreases with the ADA oxidation degree, **b** the gelation time of 10% oxidized ADA increases with the increase in the ratio of ADA/GEL

of bioplotter was set at 10 °C for all groups throughout the printing process.

Crosslinking degree

Crosslinking of ADA and GEL relies on the Schiff's base formation between amino groups of GEL and the aldehyde groups of ADA. The crosslinking degree of ADA50–GEL50 hydrogels generally increases with the ADA oxidation degree, although there was no statistical significance between 10%ADA50–GEL50 and 30%ADA50–GEL50 groups (Fig. 4a). Meanwhile, the crosslinking degrees of 10%ADA hydrogel groups increase with the increase in the ratio of ADA/GEL (Fig. 4b). These results are understandable when considering that the crosslinking degree of ADA–GEL hydrogels was calculated based on the changes of moles of the reacted amino groups in this study. The more aldehyde groups were provided by ADA, and the more GEL component was consumed in the ADA–GEL hydrogels, which led to a higher calculated crosslinking degree.

Gelatin release

The gelatin release of ADA–GEL hydrogels in PBS at pH 7.4 at 37 °C was investigated (Fig. 5). Gelatin started to release immediately after immersion in PBS, and a comparatively higher amount of gelatin was released from all ADA–GEL hydrogel groups after 72 h. The gelatin release rate was high in all hydrogel groups during the initial 12 h and followed by a decreased release rate. When the oxidation degree was 10%, the release of gelatin increased with increasing gelatin concentration, which can be explained by the increasing extent of physical crosslinking. For 50%ADA–50%GEL groups, the gelatin release decreased with increasing the oxidation degree of ADA. This was probably because higher oxidation degree ADA provided more

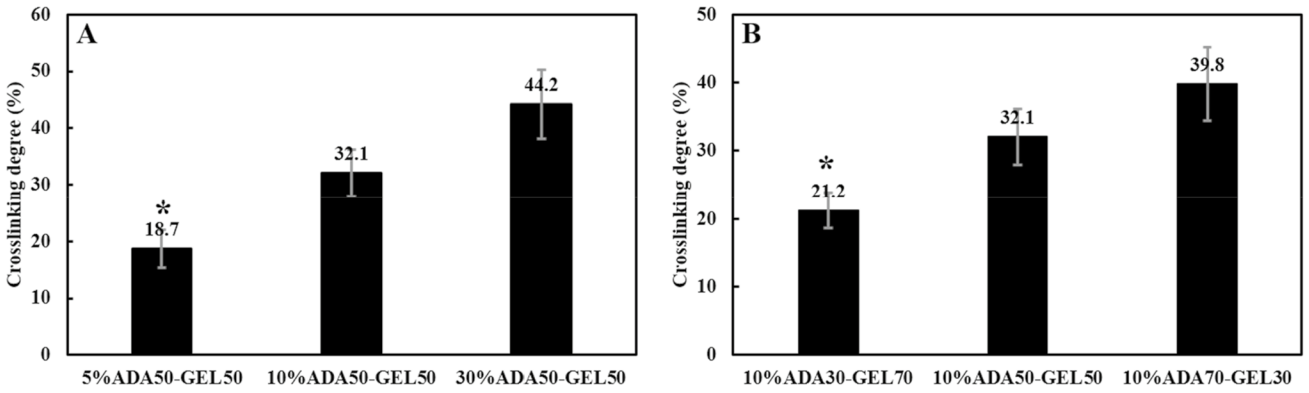

Fig. 4 Crosslinking degrees of ADA–GEL expressed as a percentage of consumed amino groups to total amino groups. **a** The crosslinking degree of ADA50–GEL50 increases with the ADA oxidation degree, **b** the crosslinking degree of 10% oxidized ADA increases with the increase in the ratio of ADA/GEL

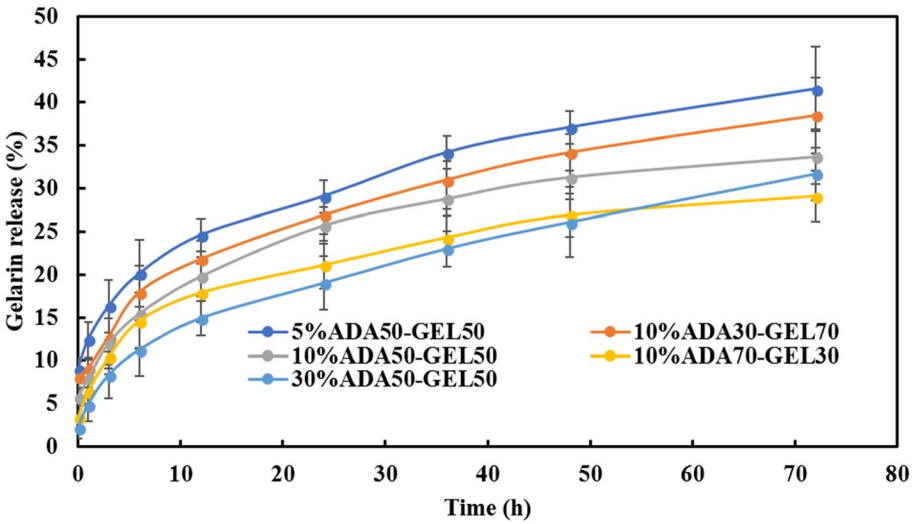

Fig. 5 Cumulative gelatin release (wt%) as a function of incubation time in PBS from printed ADA–GEL hydrogel scaffolds

active aldehyde groups leading to the increasing extent of chemical crosslinking between ADA and GEL. The GEL component typically enhances cell–material interactions due to the presence of the RGD sequence in gelatin [40, 41]. The loss of gelatin during culture was expected but not desirable since this would lead to significant cell loss. It was also observed that 30%ADA50–GEL50 showed a higher gelatin release percentage than 10%ADA70–GEL30 after 48 h of culture. This is probably because 30% of oxidized ADA cannot be efficiently crosslinked by Ca^{2+}, leading to a relative loosely crosslinked structure and more gelatin to be released.

FTIR analysis

The spectrum of 10%ADA50–GEL50 (this composition is selected to represent all compositions as all spectra show the same peaks) presents absorption bands at around 1586 and 1530 cm^{-1} due to *n*(C=N) suggesting the formation of Schiff's base [42] (Fig. 6). The band of Schiff's base at 1586 cm^{-1} is broad probably due to its overlapping with the band at 1617 cm^{-1} of amide I of uncrosslinked gelatin. There was no significant difference between pre-Ca^{2+} crosslinking ADA–GEL and post-Ca^{2+} crosslinking ADA–GEL hydrogels. Meanwhile, the amide II band at 1511 cm^{-1} of gelatin is missing in the ADA–GEL spectrum, demonstrating the involvement of amide II groups in the covalent crosslinking reaction.

Scaffold fabrication and mechanical properties

Each hydrogel group was loaded into the syringe of bioplotter and printed. Although each group showed printability to some extent, it was found that the printed structures of 5%ADA50–GEL50, 10%ADA30–GEL70, 10%ADA50–GEL50 and 30% ADA50–GEL50 were difficult to preserve. The adjacent printed strands tent to merge with each other and pores disappeared (Fig. 7).

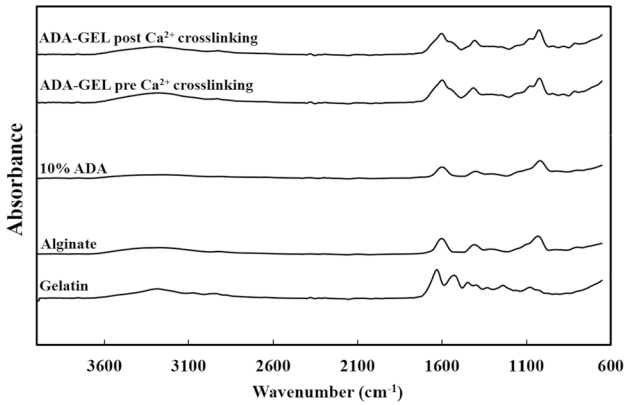

Fig. 6 FTIR spectra of gelatin, alginate, 10% oxidized ADA and ADA–GEL hydrogels

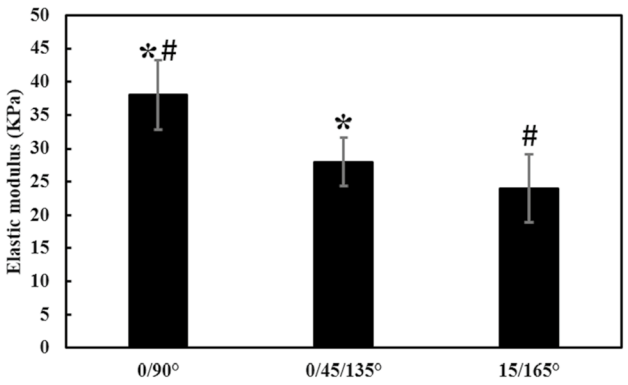

Fig. 8 Elastic modulus of 10%ADA70–GEL30 hydrogels with SO of 0°/90°, 0°/45°/135°, 15°/165° (*$p < 0.05$, $n = 3$)

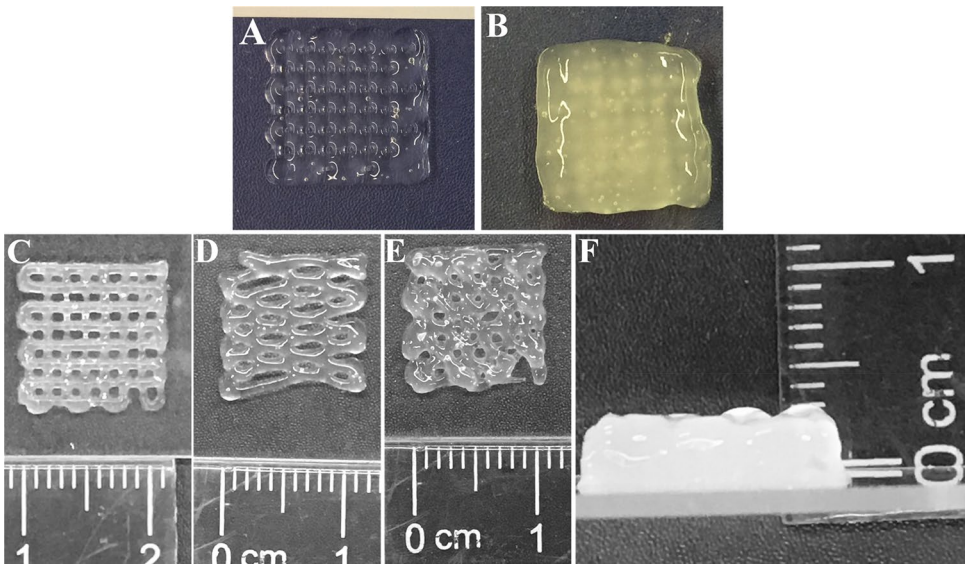

Fig. 7 Representative photographs showing the printed two-layer structure (**a**) and eight-layer construct (**b**) from hydrogel groups such as 5%ADA50–GEL50, 10%ADA30–GEL70, 10%ADA50–GEL50, 30% ADA50–GEL50, **c** top view of printed ADA–GEL hydrogel scaffolds with SO of 0°/90°, **d** 15°/165°, **e** 0°/45°/135° and **f** side view of printed hydrogel showing the height of the printed structure. 10%ADA50–GEL50 hydrogel

10%ADA70–GEL30 demonstrated the best printability among all groups and were printed with different SO of 0°/90°, 15°/165° and 0°/45°/135° (Fig. 7c–e) with a height of approximate 3 mm (Fig. 7). The influence of SO on the elastic modulus of printed hydrogels was investigated by testing the mechanical properties of 10%ADA70–GEL30 hydrogel group. 0°/90° pattern showed a significantly higher elastic modulus than that of 0°/45°/135° and 15°/165° patterns (Fig. 8).

Live/dead assay

To investigate the influence of different hydrogel formulations on cell survival, cell viability and proliferation assays were conducted on the cell-laden ADA–GEL hydrogel disks. Cell-laden 5%ALG hydrogel disks were used as a control. Embedded cells were homogenously distributed in the hydrogel disks, and live cells are predominant in these disks (Figure S7). 5%ALG hydrogel disks showed the lowest cell viability at both day 1 and 7 probably due to the high viscosity of 5% ALG hydrogel-forming solution. The cell viabilities of five experimental groups do not show a significant difference (Figure S8). There was a significant increase in cell number from day 1 to 7 for each group. At day 7, 5% ALG hydrogel group had a significantly lowest cell number, possibly because of the high viscosity of 5% ALG limited the cell proliferation.

10%ADA70–GEL30 showed the best printability among all groups. Meanwhile, the cell viability test conducted on hydrogel disks demonstrated there were not statistical difference among all ADA–GEL hydrogel groups. 10%ADA70–GEL30 hydrogel scaffolds showed the least cumulative gelatin release after 72 h culture in PBS and thus minimum cell loss was expected. Therefore, 10%ADA70–GEL30 hydrogel formulation was used to formulate bio-ink for bioprinting (Fig. 9). At day 1, embedded cells were evenly distributed, and most cells were alive. The shape of printed strands can be clearly recognized as demonstrating acceptable printability for both groups. At day 7, the width of printed 5%ALG hydrogel strands was still comparable to that of day 1 while the width of printed strands of 10%ADA70–GEL30 appeared larger and the boundaries between strands and background seemed not as clear as day 1, which was probably due to the relatively lower viscosity and gelation release of 10%ADA70–GEL30 leading to the dissolution of hydrogel during culture period. Cell viabilities of both 5%ALG and 10%ADA70–GEL30 maintained at a high level from around 70 to 90% through the culture period, with 10%ADA70–GEL30 showing statistically higher cell viability at day 7. Meanwhile, the cell number of 10%ADA70–GEL30 was significantly higher than 5%ALG group (Fig. 10). This suggested that 10%ADA70–GEL30 hydrogel scaffold provided a more favorable microenvironment for embedded cells, which could be due to its relative lower viscosity and the addition of bioactive GEL.

The addition of GEL promoted the bioactivity and provided cell adhesion sites for the formulated bio-inks, and this was verified by the phalloidin staining of EA.hy926 cell-laden hydrogel scaffolds (Fig. 11). After 7 days of culture, phalloidin F-actin stained cells indicated the cellular morphology difference between two groups. Some EA.hy926 cells seemed attached and elongated in 10%ADA70–GEL30 hydrogel matrix (Fig. 11a, b), while the cells were still round and unattached in the 5%ALG matrices (Fig. 11c). It has been also found that the printed scaffold has been losing

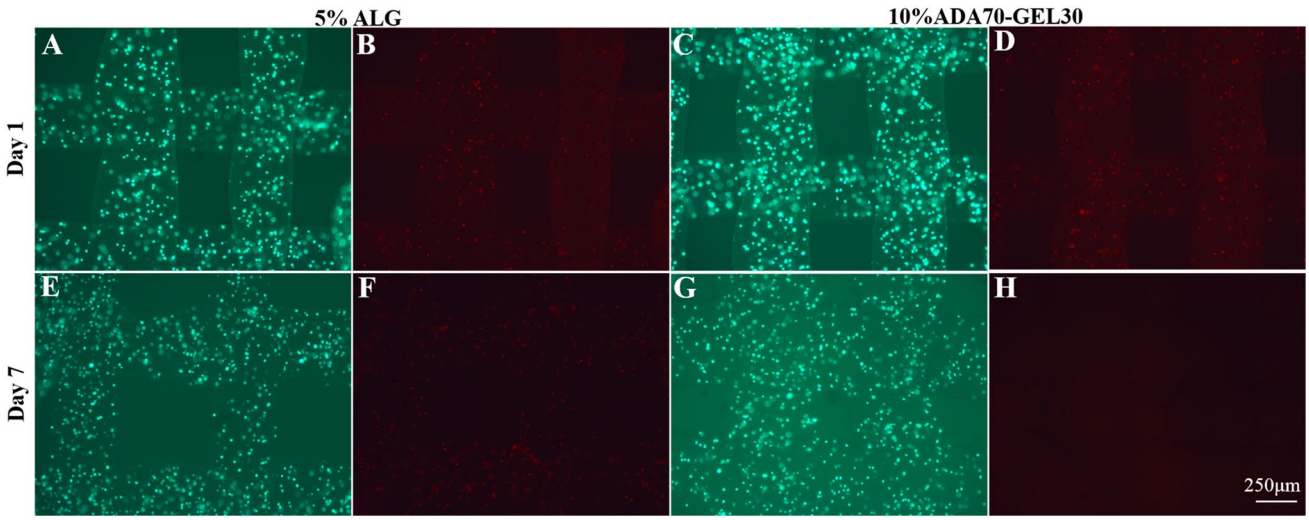

Fig. 9 Fluorescent images of the bioprinted EA.hy926 cell-laden hydrogel scaffolds showing live (green) and dead (red) cells at day 1 (**a**–**d**) and 7 (**e**–**h**) for 5%ALG (**a**, **b**, **e**, **f**) and 10%ADA70–GEL30 (**c**, **d**, **g**, **h**)

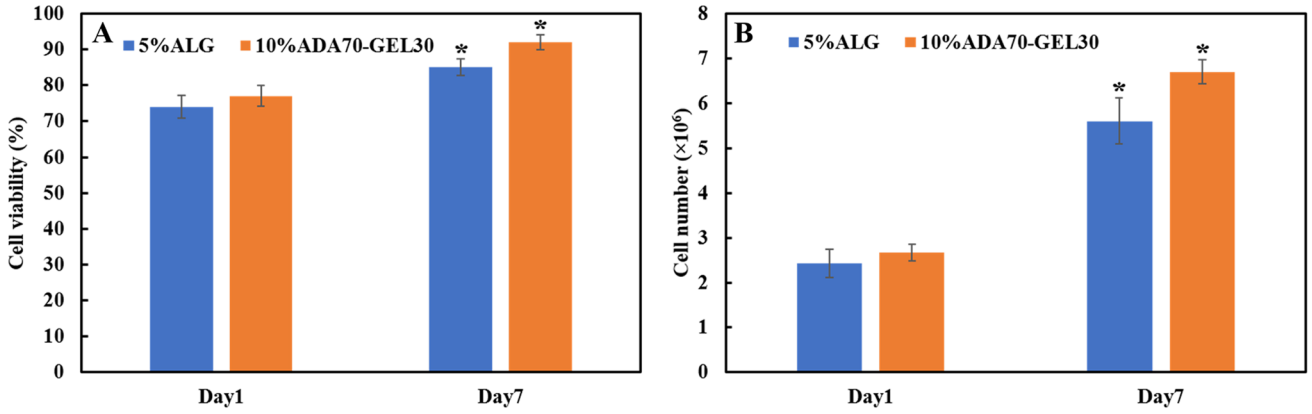

Fig. 10 Cell viability (**a**) and cell number (**b**) of fabricated hydrogel disks on day 1 and day 7 for all hydrogel groups. (*$p < 0.05$, $n = 3$)

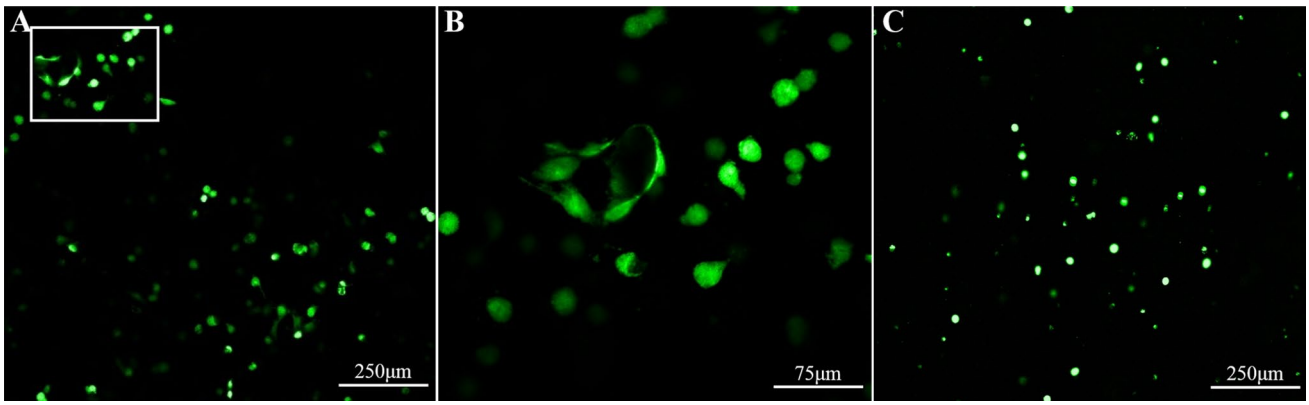

Fig. 11 Confocal laser scanning microscopy of phalloidin-stained EA.hy926 cell-laden hydrogel scaffolds after 7 days of culture: **a** 10%ADA70–GEL30, **b** enlarged photograph of the box area in (**a**), **c** 5% ALG

its mechanical stability during culture, which is probably because the crosslinked printed structure lost crosslinking agents and partial uncrosslinked GEL component during regular culture medium changes.

Conclusions

Engineering cell-laden cardiac patches to renew the loss of cells caused by MI has attracted much attention for MI treatment, but fabrication of porous cell-laden patches remains challenging owing to the limitations of currently available hydrogels and their processing techniques. In the present study, a bio-ink from ADA and GEL was formulated and characterized in terms of printability, mechanical and biological properties. Specifically, by varying ADA oxidation degree and ADA-to-GEL ratio, various bio-inks were formulated and among them, one of the ADA with an oxidation degree of 10% and a concentration ratio of 70/30 (or 10%ADA70–GEL30) demonstrated the best printability among the groups examined. Furthermore, the biocompatibility of the bio-ink formulation and bioprinting process was examined and characterized by bioprinting EA.hy926 cell-laden ADA–GEL hydrogel scaffolds, with the results illustrating their potential applications in MI repair.

Acknowledgements Financial Support from the University of Saskatchewan via scholarship and the Natural Science and Engineering Research Council of Canada via the Discovery Grant is acknowledged.

Compliance with ethical standards

Conflict of interest The authors declare that there is no conflict of interest.

Ethical approval This study does not contain any studies with human or animal subjects performed by any of the authors.

References

1. van Rooij E (2016) Cardiac repair after myocardial infarction. N Engl J Med. https://doi.org/10.1056/nejmcibr1512011
2. Okamoto T, Akaike T, Sawa T, Miyamoto Y, Van der Vliet A, Maeda H (2001) Activation of matrix metalloproteinases by peroxynitrite-induced protein S-glutathiolation via disulfide S-oxide formation. J Biol Chem. https://doi.org/10.1074/jbc.M102417200
3. Fert-Bober J, Leon H, Sawicka J et al (2008) Inhibiting matrix metalloproteinase-2 reduces protein release into coronary effluent from isolated rat hearts during ischemia-reperfusion. Basic Res Cardiol. https://doi.org/10.1007/s00395-008-0727-y
4. Qun Gao C, Sawicki G, Suarez-Pinzon WL et al (2003) Matrix metalloproteinase-2 mediates cytokine-induced myocardial contractile dysfunction. Cardiovasc Res. https://doi.org/10.1016/S0008-6363(02)00719-8
5. Doroszko A, Polewicz D, Sawicka J, Richardson JS, Sawicki G, Cheung PY (2009) Cardiac dysfunction in an animal model of neonatal asphyxia is associated with increased degradation of MLC1 by MMP-2. Basic Res Cardiol. https://doi.org/10.1007/s00395-009-0035-1
6. Bozkurt B, Kribbs SB, Clubb FJ et al (1998) Pathophysiologically relevant concentrations of tumor necrosis factor-α promote progressive left ventricular dysfunction and remodeling in rats. Circulation. https://doi.org/10.1161/01.CIR.97.14.1382
7. Ye KY, Black LD (2011) Strategies for tissue engineering cardiac constructs to affect functional repair following myocardial infarction. J Cardiovasc Transl Res. https://doi.org/10.1007/s12265-011-9303-1
8. Segers VFM, Lee RT (2010) Protein therapeutics for cardiac regeneration after myocardial infarction. J Cardiovasc Transl Res. https://doi.org/10.1007/s12265-010-9207-5
9. Fang R, Tian W, Chen X (2017) Synthesis of injectable alginate hydrogels with muscle-derived stem cells for potential myocardial infarction repair. Appl Sci. https://doi.org/10.3390/app7030252
10. Bai X, Fang R, Zhang S et al (2013) Self-cross-linkable hydrogels composed of partially oxidized alginate and gelatin for myocardial infarction repair. J Bioact Compat Polym. https://doi.org/10.1177/0883911512473230
11. Izadifar M, Chapman D, Babyn P, Chen X, Kelly ME (2018) UV-assisted 3D bioprinting of nanoreinforced hybrid cardiac patch for myocardial tissue engineering. Tissue Eng Part C Methods. https://doi.org/10.1089/ten.tec.2017.0346
12. Izadifar M, Babyn P, Kelly ME, Chapman D, Chen X (2017) Bioprinting pattern-dependent electrical/mechanical behavior of cardiac alginate implants: characterization and ex vivo phase-contrast microtomography assessment. Tissue Eng Part C Methods. https://doi.org/10.1089/ten.tec.2017.0222
13. Shi C, Li Q, Zhao Y et al (2011) Stem-cell-capturing collagen scaffold promotes cardiac tissue regeneration. Biomaterials 32(10):2508–2515. https://doi.org/10.1016/j.biomaterials.2010.12.026
14. You F, Eames BF, Chen X (2017) Application of extrusion-based hydrogel bioprinting for cartilage tissue engineering. Int J Mol Sci 18(7):1597. https://doi.org/10.3390/ijms18071597
15. Chen DXB (2019) Extrusion bioprinting of scaffolds for tissue engineering applications. Springer, Cham
16. Naghieh S, Sarker M, Izadifar M, Chen X (2018) Dispensing-based bioprinting of mechanically-functional hybrid scaffolds with vessel-like channels for tissue engineering applications—a brief review. J Mech Behav Biomed Mater. https://doi.org/10.1016/j.jmbbm.2017.11.037
17. Ning L, Chen X (2017) A brief review of extrusion-based tissue scaffold bio-printing. Biotechnol J. https://doi.org/10.1002/biot.201600671
18. Nelson TJ, Martinez-Fernandez A, Yamada S, Perez-Terzic C, Ikeda Y, Terzic A (2009) Repair of acute myocardial infarction by human stemness factors induced pluripotent stem cells. Circulation 120(5):408–416. https://doi.org/10.1161/CIRCULATIONAHA.109.865154
19. Axpe E, Oyen ML (2016) Applications of alginate-based bioinks in 3D bioprinting. Int J Mol Sci. 17(12):1976. https://doi.org/10.3390/ijms17121976
20. You F, Wu X, Chen X (2017) 3D printing of porous alginate/gelatin hydrogel scaffolds and their mechanical property characterization. Int J Polym Mater Polym Biomater 66(6):299–306. https://doi.org/10.1080/00914037.2016.1201830
21. You F, Wu X, Zhu N, Lei M, Eames BF, Chen X (2016) 3D printing of porous cell-laden hydrogel constructs for potential applications in cartilage tissue engineering. In: ACS biomaterials science & engineering, vol 2, pp 1200–1210
22. Al-Shamkhani A, Duncan R (1995) Radioiodination of alginate via covalently-bound tyrosinamide allows monitoring of its fate in vivo. J Bioact Compat Polym 10(1):4–13. https://doi.org/10.1177/088391159501000102
23. Balakrishnan B, Lesieur S, Labarre D, Jayakrishnan A (2005) Periodate oxidation of sodium alginate in water and in ethanol–water mixture: a comparative study. Carbohydr Res 340(7):1425–1429. https://doi.org/10.1016/j.carres.2005.02.028
24. Lee KY, Mooney DJ (2012) Alginate: properties and biomedical applications. Prog Polym Sci 37(1):106–126. https://doi.org/10.1016/j.progpolymsci.2011.06.003.Alginate
25. Chan BP, Leong KW (2008) Scaffolding in tissue engineering: general approaches and tissue-specific considerations. Eur Spine J 17:467–479. https://doi.org/10.1007/s00586-008-0745-3
26. Rahmany MB, Van Dyke M (2013) Biomimetic approaches to modulate cellular adhesion in biomaterials: a review. Acta Biomater 9(3):5431–5437. https://doi.org/10.1016/j.actbio.2012.11.019
27. Balakrishnan B, Joshi N, Jayakrishnan A, Banerjee R (2014) Self-crosslinked oxidized alginate/gelatin hydrogel as injectable, adhesive biomimetic scaffolds for cartilage regeneration. Acta Biomater 10(8):3650–3663. https://doi.org/10.1016/j.actbio.2014.04.031
28. Pok S, Myers JD, Madihally SV, Jacot JG (2013) A multilayered scaffold of a chitosan and gelatin hydrogel supported by a PCL core for cardiac tissue engineering. Acta Biomater 9(3):5630–5642. https://doi.org/10.1016/j.actbio.2012.10.032
29. Fang R, Qiao S, Liu Y et al (2015) Sustained co-delivery of BIO and IGF-1 by a novel hybrid hydrogel system to stimulate endogenous cardiac repair in myocardial infarcted rat hearts. Int J Nanomed. https://doi.org/10.2147/IJN.S81451
30. Sarker B, Papageorgiou DG, Silva R et al (2014) Fabrication of alginate–gelatin crosslinked hydrogel microcapsules and evaluation of the microstructure and physico-chemical properties. J Mater Chem B 2(11):1470. https://doi.org/10.1039/c3tb21509a
31. Gomez CG, Rinaudo M, Villar MA (2007) Oxidation of sodium alginate and characterization of the oxidized derivatives. Carbohydr Polym 67(3):296–304. https://doi.org/10.1016/j.carbpol.2006.05.025
32. Zuidema JM, Rivet CJ, Gilbert RJ, Morrison FA (2014) A protocol for rheological characterization of hydrogels for tissue engineering strategies. J Biomed Mater Res Part B Appl Biomater 102(5):1063–1073. https://doi.org/10.1002/jbm.b.33088
33. Vasconcelos A, Gomes AC, Cavaco-Paulo A (2012) Novel silk fibroin/elastin wound dressings. Acta Biomater 8(8):3049–3060. https://doi.org/10.1016/j.actbio.2012.04.035
34. Peterson GL (1977) A simplification of the protein assay method of Lowry et al. which is more generally applicable. Anal Biochem 83(2):346–356. https://doi.org/10.1016/0003-2697(77)90043-4

35. Balakrishnan B, Jayakrishnan A (2005) Self-cross-linking biopolymers as injectable in situ forming biodegradable scaffolds. Biomaterials 26(18):3941–3951. https://doi.org/10.1016/j.biomaterials.2004.10.005
36. Lee HJ, Ahn SH, Kim GH (2012) Three-dimensional collagen/alginate hybrid scaffolds functionalized with a drug delivery system (DDS) for bone tissue regeneration. Chem Mater. 24(5):881–891. https://doi.org/10.1021/cm200733s
37. Vieira EFS, Cestari AR, Airoldi C, Loh W (2008) Polysaccharide-based hydrogels: preparation, characterization, and drug interaction behaviour. Biomacromol 9(4):1195–1199. https://doi.org/10.1021/bm7011983
38. Smitha B, Sridhar S, Khan AA (2005) Chitosan–sodium alginate polyion complexes as fuel cell membranes. Eur Polym J 41(8):1859–1866. https://doi.org/10.1016/j.eurpolymj.2005.02.018
39. Kang HA, Shin MS, Yang JW (2002) Preparation and characterization of hydrophobically modified alginate. Polym Bull 47(5):429–435. https://doi.org/10.1007/s002890200005
40. Wu SC, Chang WH, Dong GC, Chen KY, Chen YS, Yao CH (2011) Cell adhesion and proliferation enhancement by gelatin nanofiber scaffolds. J Bioact Compat Polym 26(6):565–577. https://doi.org/10.1177/0883911511423563
41. Rosellini E, Cristallini C, Barbani N, Vozzi G, Giusti P (2009) Preparation and characterization of alginate/gelatin blend films for cardiac tissue engineering. J Biomed Mater Res Part A 91A(2):447–453. https://doi.org/10.1002/jbm.a.32216
42. Ye J, Xiong J, Sun R (2012) The fluorescence property of Schiff's bases of carboxymethyl cellulose. Carbohydr Polym 88(4):1420–1424. https://doi.org/10.1016/j.carbpol.2012.02.030